

Spin Correlations in $\text{Ho}_2\text{Ti}_2\text{O}_7$: a Dipolar Spin Ice System

S.T. Bramwell¹, M.J. Harris², B.C. den Hertog³, M.J.P. Gingras^{3,4}, J.S. Gardner⁵, D.F. McMorrow⁶, A.R. Wildes⁷,
A.L. Cornelius⁸, J.D.M. Champion¹, R.G. Melko³ and T. Fennell¹

¹*Department of Chemistry, University College London, 20 Gordon Street, London, WC1H 0AJ, United Kingdom*

²*ISIS Facility, Rutherford Appleton Laboratory, Chilton, Didcot, Oxfordshire OX11 0QX, United Kingdom*

³*Department of Physics, University of Waterloo, Ontario, Canada N2L 3G1*

⁴*Canadian Institute for Advanced Research, 180 Dundas Street W., Toronto, Ontario, Canada M5G 1Z8*

⁵*National Research Council, NPMR, Chalk River Laboratories, Chalk River, Ontario, Canada K0J 1J0*

⁶*Condensed Matter Physics and Chemistry Department, Risø National Laboratory, DK-4000 Roskilde, Denmark*

⁷*Institut Laue-Langevin, 156X, 38042 Grenoble Cedex, France*

⁸*Department of Physics, University of Nevada, Las Vegas, Nevada, 89154-4002*

(May 28, 2018)

The pyrochlore material $\text{Ho}_2\text{Ti}_2\text{O}_7$ has been suggested to show “spin ice” behaviour. We present neutron scattering and specific heat results that establish unambiguously that $\text{Ho}_2\text{Ti}_2\text{O}_7$ exhibits spin ice correlations at low temperature. Diffuse magnetic neutron scattering from $\text{Ho}_2\text{Ti}_2\text{O}_7$ is found to be quite well described by a nearest neighbour spin ice model and very accurately described by a dipolar spin ice model. The heat capacity is well accounted for by the sum of a dipolar spin ice contribution and an expected nuclear spin contribution, known to exist in other Ho^{3+} salts. These results settle the question of the nature of the low temperature spin correlations in $\text{Ho}_2\text{Ti}_2\text{O}_7$ for which contradictory claims have been made.

Spin ice materials [1,2] are magnetic substances in which the atomic magnetic moments obey the same ordering rules as the hydrogen atoms in ice, H_2O . They provide a bridge between the simple statistical mechanics of ice-type models [3], and the complex behavior of frustrated magnets [4–7], with wider relevance to diverse areas of research such as high temperature superconductivity and neural networks. Furthermore, relatives of spin ice such as $\text{R}_2\text{Mo}_2\text{O}_7$ (R = rare earth) are a current focus of attention for their interesting electronic properties [8,9]. It is therefore important and desirable to establish the detailed physics of the simplest spin ice materials, which provide among the best model systems for the study of frustration and its broad consequences.

Experiments on $\text{Ho}_2\text{Ti}_2\text{O}_7$ provided the original motivation for the concept of spin ice [1]. In cubic $\text{Ho}_2\text{Ti}_2\text{O}_7$, (space group $Fd\bar{3}m$), the magnetic Ho^{3+} ions occupy a cubic pyrochlore lattice, a corner-linked array of tetrahedra that is identical to the lattice formed by the mid-points of the oxygen-oxygen bonds of cubic ice [10]. The ground state of Ho^{3+} is an effective Ising doublet of local $\langle 111 \rangle$ quantization axis [1,11–14], with nearest neighbor Ho^{3+} moments experiencing an overall ferromagnetic coupling that is largely dipolar in origin. Qualitatively, $\text{Ho}_2\text{Ti}_2\text{O}_7$ thus approximates the nearest neighbor spin ice model [1,15,16], in which ferromagnetically-coupled Ising spins on the pyrochlore lattice lie parallel to the local $\langle 111 \rangle$ axes that point towards the centers of the tetrahedra. The ground state of this model requires two spins pointing into and two pointing out of each tetrahedron. Then if spins represent hydrogen atom displacement vectors, one obtains the ice rules that lead to Pauling’s result for the extensive zero temperature entropy of the disordered ground state of ice [10,17].

Neutron scattering experiments on $\text{Ho}_2\text{Ti}_2\text{O}_7$ in zero

magnetic field show only broad diffuse scattering down to a temperature $T \sim 0.35$ K, consistent with a disordered spin ice state [1,18], while low temperature muon spin relaxation (μSR) work also finds no evidence for a magnetic transition [18]. Field-induced ordered states are also consistent with the spin ice scenario [1,15]. Combined with a ferromagnetic Curie-Weiss temperature of $\theta_{CW} = 1.9 \pm 0.1$ K, $\text{Ho}_2\text{Ti}_2\text{O}_7$ would thus appear to be a prototypical spin ice material. Another candidate for spin ice behaviour is $\text{Dy}_2\text{Ti}_2\text{O}_7$ [2], for which specific heat measurements down to 250 mK can be integrated to give the residual entropy expected for the spin ice model. However, none of the measurements reported in Ref. [1] or Ref. [2] constitute a proof that the spin ice ground state exists in these materials in zero applied field. Moreover, a certain amount of confusion has recently arisen due to some contradictory observations: Siddharthan *et al.* suggested that the specific heat behaviour of $\text{Ho}_2\text{Ti}_2\text{O}_7$ possibly indicates a transition to a partially ordered state at ~ 0.8 K [19], in disagreement with the neutron scattering and μSR results [1,18]. In this Letter we present neutron scattering and new heat capacity data that unambiguously establish the spin ice nature of the zero field spin correlations in $\text{Ho}_2\text{Ti}_2\text{O}_7$.

The diffuse magnetic neutron scattering from a flux grown single crystal of $\text{Ho}_2\text{Ti}_2\text{O}_7$ was measured in the static approximation on the PRISMA spectrometer at ISIS. The crystal was oriented with $[1, -1, 0]$ vertical such that the (h, h, l) scattering plane included the three principal symmetry axes $[1, 0, 0]$, $[1, 1, 0]$ and $[1, 1, 1]$. Figure 1a shows the scattering pattern at $T \sim 50$ mK. One of the main features of the experimental data is the ‘four-leaf clover’ of intense scattering around $(0, 0, 0)$. There is also strong scattering around $(0, 0, 3)$ and a broad region of slightly weaker scattering around $(3/2, 3/2, 3/2)$.

These intense regions are connected by narrow necks of intensity giving the appearance of bow-ties. The width of the intense regions indicates short range correlations on the order of one lattice spacing. Qualitatively similar scattering has been observed in ice itself [20].

To model this data we use the standard expression for the neutron scattered intensity $I(\mathbf{q})$ [21], along with the Hamiltonian [22–24]:

$$H = -J \sum_{\langle ij \rangle} \mathbf{S}_i^{z_i} \cdot \mathbf{S}_j^{z_j} + D r_{nn}^3 \sum_{i>j} \frac{\mathbf{S}_i^{z_i} \cdot \mathbf{S}_j^{z_j}}{|\mathbf{r}_{ij}|^3} - \frac{3(\mathbf{S}_i^{z_i} \cdot \mathbf{r}_{ij})(\mathbf{S}_j^{z_j} \cdot \mathbf{r}_{ij})}{|\mathbf{r}_{ij}|^5}, \quad (1)$$

where Ising spins $\mathbf{S}_i^{z_i}$ of unit length are constrained to their local $z_i = \langle 1, 1, 1 \rangle$ axes; J is a near neighbor exchange coupling and D the dipolar coupling. Because of the local Ising axes the effective nearest neighbor energy scales are $J_{nn} \equiv J/3$ and $D_{nn} \equiv 5D/3$ [24].

The near neighbor spin ice model [1,16] corresponds to $D = 0$ and J positive (ferromagnetic). Data were simulated with 3456 spins ($6 \times 6 \times 6$ cubic unit cells) at $T/J = 0.15$ where the model is effectively in an ice-rules ground state. The calculated pattern is shown in Fig. 1b. It successfully reproduces the main features of the experimental pattern, but there are differences, notably in the extension of the $(0, 0, 0)$ intense region along (h, h, h) and the relative intensities of the regions around $(0, 0, 3)$ and $(3/2, 3/2, 3/2)$. Also, the experimental data shows much broader regions of scattering along the diagonal directions. Clearly, the experimental spin correlations do not reflect a completely disordered arrangement of ice-rule states, but some states are favored over others [23,24].

The more complete dipolar spin ice model [22–24], has $D_{nn} = 2.35$ K, fixed by the lattice constant, and $J_{nn} = -0.52$ K a negative (antiferromagnetic) parameter determined by fitting the peak temperature of the electronic magnetic heat capacity (see below). Spin ice behavior emerges in this model from the dominant effect of the long-range nature of dipolar interactions [22–24], and can quantitatively account for the heat capacity data of $\text{Dy}_2\text{Ti}_2\text{O}_7$ (taken from Ref. [2]) [22,23]. Using single spin flip dynamics, $I(\mathbf{q})$ was calculated [21] on a system size of 1024 spins ($4 \times 4 \times 4$), at $T = 0.6$ K where significant ground state correlations have developed, using standard Ewald summation techniques which properly handle infinite summation of dipole-dipole energy terms (see Refs. [22,23]). The calculated pattern is shown in Fig 1c. It captures most details of the experimental pattern missed by the near neighbor spin ice model in Fig. 1b, such as the four intense regions around $(0, 0, 0)$, the relative intensities of the regions around $(0, 0, 3)$ and $(3/2, 3/2, 3/2)$ and the spread of the broad features along the diagonal. Note also the low scattering intensity at $(2, 2, 0)$, consistent with the experimental low intensity around at $(2, 2, 0)$. The approach of $I(\mathbf{q})$ to zero at $q = 0$ is consistent with a recent observation that the ac-susceptibility of $\text{Ho}_2\text{Ti}_2\text{O}_7$ approaches zero below 0.7 K [25].

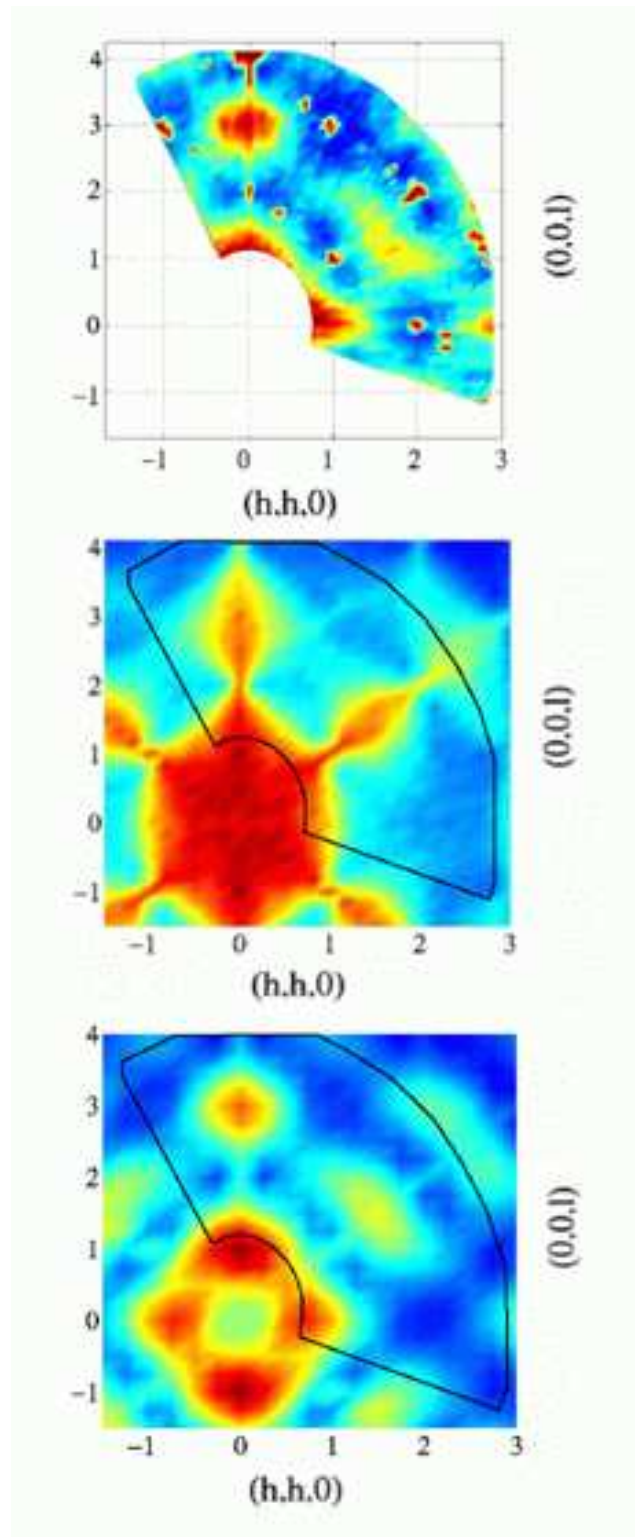


FIG. 1. (a) Experimental neutron scattering pattern of $\text{Ho}_2\text{Ti}_2\text{O}_7$ in the (hhl) plane of reciprocal space at $T \sim 50$ mK. Dark blue shows the lowest intensity level, red-brown the highest. Temperature dependent measurements have shown that the sharp diffraction spots in the experimental pattern are nuclear Bragg peaks with no magnetic component. (b) $I(\mathbf{q})$ for the nearest neighbor spin ice model at $T = 0.15J$. (c) $I(\mathbf{q})$ for the dipolar spin ice model at $T = 0.6$ K. The areas defined by the solid lines denote the experimental data region of (a).

The difference between Figs. 1b and 1c shows that dipolar interactions, whilst inducing a low energy ice-rules manifold, do cause further correlations to emerge among the spins than those that are due to a nearest neighbor ferromagnetic interaction. This thermal bias towards certain ice-rule configurations in the dipolar model is consistent with mean field calculations [24], and also with the behavior observed when single spin flip algorithms in numerical simulations [23]. In that case, the intense regions of $I(\mathbf{q})$ evolve into Bragg peaks upon cooling below 0.17 K as the system enters a long range ordered state. It may be that at low temperature in $\text{Ho}_2\text{Ti}_2\text{O}_7$, short range correlations associated with a putative ordered state begin to emerge, but are dynamically inhibited from developing into Bragg peaks upon further cooling.

To further test the dipolar model, we show in Fig. 2 a comparison between the calculated $I(\mathbf{q})$ and that measured in a separate experiment with the same crystal on the IN14 spectrometer at the ILL, Grenoble. Here it was found that the diffuse scattering was nearly temperature-independent below 0.7 K. For the theoretical fit, the form factor was determined empirically by fitting the neutron data at 35 K in the paramagnetic regime [26]. The comparison between theory and experiment obtained at 0.7 K along $(0, 0, l)$ is shown in Fig. 2a, where it is seen to be very satisfactory. Hence it is clear that the dipolar Hamiltonian (1) describes the magnetic behaviour of $\text{Ho}_2\text{Ti}_2\text{O}_7$ to a very good approximation.

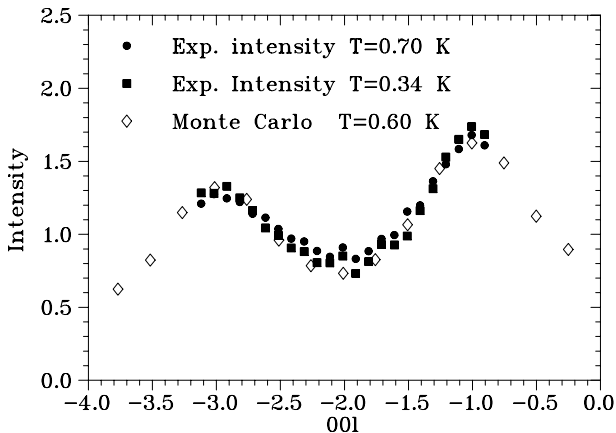


FIG. 2. Experimental neutron scattering intensity, $I(\mathbf{q})$, of $\text{Ho}_2\text{Ti}_2\text{O}_7$ (filled symbols) along the $(00l)$ direction of reciprocal space. For quantitative comparison is the intensity (open symbols) obtained from Monte Carlo simulation of the dipolar spin ice model with $J_{nn} = -0.52$ K and $D_{nn} = 2.35$ K.

We now turn to the heat capacity, analysis of which is complicated by the previously reported difficulty in equilibrating this material at low temperatures ($T < 0.8$ K) [19]. Single crystals of $\text{Ho}_2\text{Ti}_2\text{O}_7$ were synthesized using the floating-zone method described in [27]. Heat capacity measurements were performed in a Quantum Design PPMS system inside a 9T superconducting magnet. The heat capacity was measured using a thermal relaxation

method between 0.34 and 20 K. Good thermal contact between the single crystal and sample stage was ensured with the uses of low temperature grease. Our heat capacity data, shown in Fig. 3, go to lower temperature than those of Ref. [19] and show no evidence for a phase transition. Rather, there is a noticeable change in dynamics as equilibration times become longer deep within the spin ice regime, as signaled by the vanishing electronic specific heat capacity, but the total heat capacity continues to steadily increase as the temperature is lowered (note, however, the shoulder at $T \sim 1.5$ K).

Blöte *et al.* measured the heat capacity of the pyrochlore $\text{Ho}_2\text{GaSbO}_7$ [11] and obtained similar behavior to that found for $\text{Ho}_2\text{Ti}_2\text{O}_7$. They successfully accounted for the heat capacity below ~ 2 K by introducing a Schottky anomaly with a theoretical maximum for Ho ($I = 7/2$) of 0.9 R, due to a splitting of the eight nuclear levels with a level spacing of 0.3 K.

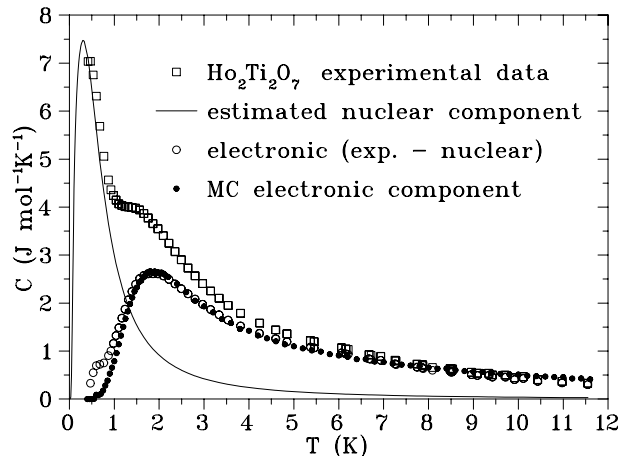


FIG. 3. The total specific heat of $\text{Ho}_2\text{Ti}_2\text{O}_7$ is shown by the empty squares. Expected nuclear contribution is indicated by the line, while the electronic contribution has been estimated by subtracting these two curves (open circles). Near 0.7 K this subtraction is prone to a large error (see text). Dipolar spin ice simulation results are indicated by the filled circles.

The electronic component of the magnetic heat capacity for $\text{Ho}_2\text{Ti}_2\text{O}_7$ may be extracted by subtracting off the nuclear Schottky contribution estimated by Blöte *et al.* for $\text{Ho}_2\text{GaSbO}_7$ [11]. This reveals an electronic magnetic heat capacity that shows the same characteristic spin ice shape as observed for $\text{Dy}_2\text{Ti}_2\text{O}_7$ [2]. Fig. 3 shows a very broad electronic magnetic peak centered at $T \sim 1.9$ K. With this heat capacity revealed, a natural explanation of the observed change in dynamics in this material at $T \sim 0.8$ K, (attributed to a transition in Refs. [19,28]), is that this is approximately the temperature below which macroscopic relaxation of the magnetic degrees of freedom into the low energy ice-rule manifold has essentially ceased (this is also consistent with Ref. ([25])). In other words, the onset of spin ice physics is much higher than this temperature, most likely $T \sim 1.9$ K. The behavior of $\text{Ho}_2\text{Ti}_2\text{O}_7$ may be compared to that of $\text{Dy}_2\text{Ti}_2\text{O}_7$, where the onset of spin ice correlations (peak in the specific

heat) is ~ 1.2 K and the magnetic heat capacity is almost zero at $T \sim 0.25$ K [2].

The subtraction of the nuclear contribution, itself an approximation, becomes prone to error in the range 0.6-0.9 K where the nuclear specific heat rises sharply. Hence, although our subtraction reveals a small feature in the electronic specific heat at $T \sim 0.7$ K, a subtraction of the nuclear contribution from the total heat capacity data reported in Ref. [19] gives no such feature; thus we conclude that an electronic-only heat capacity in this region cannot be reliably determined.

Based on the electronic specific heat peak height, and the temperature at which it occurs, the dipolar spin ice model allows two independent methods for determining the value of the nearest neighbor exchange for $\text{Ho}_2\text{Ti}_2\text{O}_7$ [22]. Using these procedures we find a nearest neighbor exchange $J_{\text{nn}} \sim -0.52$ K. In Fig. 3 we show specific heat results from a standard Monte Carlo single spin flip simulation of the dipolar spin ice model, for a system size of $6 \times 6 \times 6$ unit cells (3456 spins) with interaction parameters $J_{\text{nn}} = -0.52$ K and nearest neighbor dipole strength $D_{\text{nn}} = 2.35$ K. We find quantitative agreement between the experimental electronic specific heat, C , and that found from the simulation. At high temperature, C approaches the dipolar spin ice heat capacity smoothly, as it should since the nuclear contribution is negligible. At low T it follows the nuclear contribution once the electronic component has died. Finally, in-between the low T and high T regimes, there is the shoulder at $T \sim 1.5$ K in the total $C(T)$ (alluded to above) corresponding to a shift of regime between the dipolar spin ice controlled regime and the nuclear hyperfine one.

Taken with our neutron scattering results, it appears clear that $\text{Ho}_2\text{Ti}_2\text{O}_7$ is quantitatively well characterized by the dipolar spin ice model with a missing entropy close to Pauling's prediction, and what is found for $\text{Dy}_2\text{Ti}_2\text{O}_7$ [2,22]. The spin ice behavior revealed explicitly here for $\text{Ho}_2\text{Ti}_2\text{O}_7$ is in contrast to the conclusions of Refs. [19,28]. These were based on a finite size truncation of the dipolar interaction in the simulations and only a qualitative comparison with experimental specific heat that neglected the important nuclear contribution (Fig. 3 of [19]). Our deduced value of the antiferromagnetic exchange interaction indicates that $\text{Ho}_2\text{Ti}_2\text{O}_7$ is further into the dipolar spin ice region of the magnetic phase diagram [22] than is $\text{Dy}_2\text{Ti}_2\text{O}_7$, contrary to the claims of Ref. [28], with $J_{\text{nn}}^{\text{Ho}}/D_{\text{nn}}^{\text{Ho}} \sim -0.22$ and $J_{\text{nn}}^{\text{Dy}}/D_{\text{nn}}^{\text{Dy}} \sim -0.53$.

In conclusion, we have unambiguously established that $\text{Ho}_2\text{Ti}_2\text{O}_7$ possesses a spin ice state in zero field. Experiments investigating the spin correlations of $\text{Dy}_2\text{Ti}_2\text{O}_7$ are in progress [29]. The Ho salt, in contrast to its Dy analogue, contains a single rare earth isotope that lends itself well to neutron scattering and the study of hyperfine effects. With intriguing spin dynamics and field-induced ordering phenomena, $\text{Ho}_2\text{Ti}_2\text{O}_7$ offers much new physics to be explored in the field of frustrated magnetism.

M.G. acknowledges financial support from NSERC of Canada, Research Corporation and the Province of On-

tario. We thank B. Fåk, P.C.W. Holdsworth, and O.A. Petrenko for useful discussions.

-
- [1] M. J. Harris, *et al.*, Phys. Rev. Lett. **79**, 2554 (1997).
 - [2] A. P. Ramirez *et al.*, Nature **399**, 333 (1999).
 - [3] E. H. Lieb and F. Y. Wu, *Phase Transitions and Critical Phenomena*, ed. C. Domb and M. S. Green, Academic Press, pp. 332-490 (1972). G. T. Barkema and M. E. J. Newman, Phys. Rev. E **57**, 1155 (1998).
 - [4] A. P. Ramirez, Ann. Rev. Mat. Sci. **24**, 453 (1994).
 - [5] J. S. Gardner *et al.*, Phys. Rev. Lett. **82**, 1012 (1999).
 - [6] R. Moessner, cond-mat/0010301.
 - [7] J.E. Greedan, "Geometrically frustrated magnetic materials". To appear in J. of Mater. Chem., (2001).
 - [8] R. Taguchi and Y. Tokura, Phys. Rev. B **60**, 10280 (1999)
 - [9] T. Katsufuji H. Y. Hwang and S-W. Cheong, Phys. Rev. Lett. **84**, 1998 (2000).
 - [10] P. W. Anderson, Phys. Rev. **102**, 1008 (1956).
 - [11] H.W.J. Blöte *et al.*, Physica **43**, 549 (1969).
 - [12] L. G. Mamsurova, K. K. Pukhov, N. G. Trusevich and L. G. Shcherbakova, Sov. Phys. Solid State, **27**, 1214 (1985).
 - [13] Y. M. Jana and D. Ghosh, Phys. Rev. B **61**, 9657 (2000).
 - [14] S. Rosenkranz *et al.*, J. Appl. Phys. **87**, 5914 (2000).
 - [15] M. J. Harris *et al.*, Phys. Rev. Lett. **81**, 4496 (1998).
 - [16] S. T. Bramwell and M. J. Harris, J. Phys.: Condens. Matter **10**, L215 1998.
 - [17] L. Pauling, J. Am. Chem. Soc. **57**, 2680 (1935).
 - [18] M. J. Harris *et al.*, J. Magn. Mag. Mat. **177-181**, 757 (1998).
 - [19] R. Siddharthan *et al.*, Phys. Rev. Lett. **83**, 1854 (1999).
 - [20] J. C. Li *et al.*, Phil. Mag. **B 69**, 1173 (1994).
 - [21] We use the following expression for the neutron scattered intensity, $I(\mathbf{q})$:
$$I(\mathbf{q}) \propto |f(q)|^2 \frac{1}{N} \sum_{ij} e^{i\mathbf{q} \cdot (\mathbf{r}_i - \mathbf{r}_j)} \langle \mathbf{S}_{i,\perp}^{z_i} \cdot \mathbf{S}_{j,\perp}^{z_j} \rangle$$
 - where $z_i = (1, 1, 1)$, $\langle \dots \rangle$ denotes a thermal average and $\mathbf{S}_{i,\perp}^{z_i}$ is the spin component at site i perpendicular to \mathbf{q} . The form factor $f(q)$ for Ho^{3+} was calculated in the small- \mathbf{q} approximation; strictly, an anisotropic form factor for the $M_J = \pm 8$ states of Ho^{3+} should be used, but the error is negligible for the comparison in Fig. 1.
 - [22] B. C. den Hertog and M. J. P. Gingras, Phys. Rev. Lett. **84**, 3430 (2000).
 - [23] R.G. Melko, B.C. den Hertog, and M.J.P. Gingras cond-mat/0009225.
 - [24] M.J.P. Gingras and B.C. den Hertog, cond-mat/0012275.
 - [25] K Matsuhira, Y. Hinatsu, K. Tenya and T. Sakakibara, J. Phys. Condens. Mat., **12** L649 (2000).
 - [26] This procedure also corrects for a small systematic temperature-independent error in the scattered intensity, believed to arise from partial masking of the observed scattering volume. The empirical form factor varied by 20% from the expected one at (0, 0, 3).
 - [27] J.S. Gardner, B. D. Gaulin and D. M^cK. Paul, J. Crystal Growth, **191**, 740 (1998).
 - [28] R. Siddharthan, B. S. Shastry and A. P. Ramirez, cond-mat/0009265.
 - [29] O.A. Petrenko, *et al.*, unpublished.